Multi-modal fission in collinear ternary cluster decay of ^{252}Cf(sf, fff)

W. von Oertzen [a,b,*], A.K. Nasirov [b,c,d], R.B. Tashkhodjaev [c,e]

[a] *Helmholtz-Zentrum Berlin, 14109 Berlin, Germany*
[b] *Joint Institute for Nuclear Research, FLNR, 141980 Dubna, Russia*
[c] *Institute of Nuclear Physics, 100214, Tashkent, Uzbekistan*
[d] *Kyungpook National University, 702-701, Daegu, Republic of Korea*
[e] *Inha University in Tashkent, 100170, Tashkent, Uzbekistan*

A B S T R A C T

We discuss the multiple decay modes of collinear fission in ^{252}Cf(sf, fff), with three fragments as suggested by the potential energy surface (PES). Fission as a statistical decay is governed by the phase space of the different decay channels, which are suggested in the PES-landscape. The population of the fission modes is determined by the minima in the PES at the scission points and on the internal potential barriers. The ternary collinear decay proceeds as a sequential process, in two steps. The originally observed ternary decay of ^{252}Cf(sf) into three different masses (e.g. $^{132-140}$Sn, $^{52-48}$Ca, $^{68-72}$Ni), observed by the FOBOS group in the FLNR (Flerov Laboratory for Nuclear Reactions) of the JINR (Dubna) the collinear cluster tripartition (CCT), is one of the ternary fission modes. This kind of "true ternary fission" of heavy nuclei has often been predicted in theoretical works during the last decades. In the present note we discuss different ternary fission modes in the same system. The PES shows pronounced minima, which correspond to several modes of ternary fragmentations. These decays have very similar dynamical features as the previously observed CCT-decays. The data obtained in the experiments on CCT allow us to extract the yields for different decay modes using specific gates on the measured parameters, and to establish multiple modes of the ternary fission decay.

1. Binary and ternary fission of ^{252}Cf

Binary fission has been observed [1] for the first time 75 years ago. Since then it has been studied intensively in the last decades, covering macroscopic and microscopic aspects of nuclear matter governing these decays. We refer to the book edited by C. Wagemans: "The Nuclear Fission Process" [2], containing a large number of articles dealing with many important aspects of this process. "Ternary fission", or light particle accompanied binary fission, with a third light particle emitted *perpendicular* to the binary fission axis has also been studied, a recent specific survey can be found in Refs. [4,5]. In these previously studied ternary decays the experiments gave decreasing yields as function of increasing mass (charge) of the third particle [5]. Already in the earlier work by Swiatecki and Strutinsky, see Refs. [6,7], it has been recognized, that ternary (and multiple) fission into fragments with comparable masses is a process, which occurs in heavy nuclei with large values of the fissility-parameter: X, for the ratios $Z^2/A > 31$, see also

Poenaru in Ref. [8] and the more recent surveys in Refs. [9–11]. In binary fission the occurrence of several decay modes is referred to as bimodal or multi-modal fission [3]. Such modes are discussed repeatedly (e.g. M.G. Itkis et al. [12]) and more recently by Ghys et al. in Ref. [13]. In this reference recent examples have been reported for a large body of data covering a larger variation (10) of the nuclear charges in the neutron deficient isotopes between gold and radium (corresponding to 20 different neutron numbers), and the decay modes are discussed.

In the present work we discuss different collinear ternary fission modes (various mass/charge partitions) in the decay of the ^{252}Cf-nucleus. The PES's (Potential Energy Surfaces, see below) are calculated for ternary collinear decays in ^{252}Cf, these show pronounced minima, which correspond to various modes of ternary fragmentations. These decays have similar dynamical features as the previously observed collinear CCT-decays. Recent experimental observations [14–16] and many earlier theoretical works have established, that in these ternary decays the collinear configuration is preferred relative to the oblate configuration. This statement holds particularly for heavy systems and for ternary fragments with larger charge, Refs. [17–19].

* Corresponding author at: Helmholtz-Zentrum Berlin, 14109 Berlin, Germany.
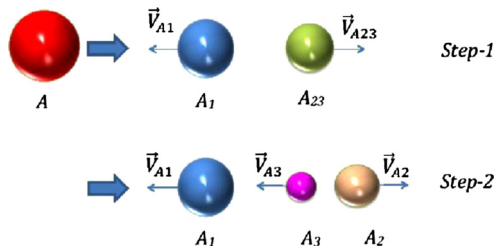*E-mail address:* oertzen@helmholtz-berlin.de (W. von Oertzen).

Fig. 1. (Color online.) Schematic illustration of collinear sequential ternary fission into three fragments of comparable mass (adopted from Ref. [24]).

The various manifestations of these ternary decay modes studied in recent years are referred to as "true ternary fission", e.g. Ref. [3], Pyatkov et al. Ref. [14] and Zagrebaev et al. in Ref. [9]. The concept of collinear decay has not been applied in previous experimental studies, in fact it was not clear how to observe a collinear ternary fission experimentally in view of the kinematical conditions (see below). Actually an experiment to detect true ternary fission with three heavier fragments with a *triangular shape of the decay-vectors* by Schall et al. [21] using several detectors covering each large (90°) angles, gave a negative result, with a lower limit of $1.0 \cdot 10^{-8}$/(binary fission).

Recent experimental studies of the decays in ^{252}Cf(sf, fff) with two fission fragment coincidences with two FOBOS-detectors [14] placed at 180°, using the *missing mass* approach, have established the phenomenon of *collinear cluster tripartition*, the CCT-decay. This new decay mode has been observed also for neutron induced fission in ^{235}U(n$_{th}$, fff), see Refs. [14–16].

This fission decay can be understood as the breakup of very (prolate deformed) elongated hyper-deformed shapes, see Ref. [20] for a discussion of hyper-deformation in ^{236}U. In this fission mode, the CCT, with the collinear decay into three fragments, the outer fragments are registered in coincidence with a missing mass [14]. In this decay mode typical fragments are isotopes (clusters, nuclei with closed shells) of Sn, Ni, and Ca. In the second paper [15], with pin-diodes, it can be seen in Fig. 7 of Ref. [15], that there is almost no background, and a high mass resolution. Therefore the Ni-bump observed in Ref. [14] is resolved into individual masses, it contains more then 20 different fragments, isotopes of mainly Ni and Ca.

The latter, Ca, as the smallest third particle, is positioned along the line connecting Sn and Ni, in this way minimizing the potential energy, and optimizing the phase space. In the experiments described in Refs. [14,15], two of the three fragments are registered. One of the intermediate fragments (see Fig. 1) moving towards one of the detectors (called arm1) are dispersed in angle, by multiple scattering, in the source backing and in the foils of the timing detector. Due to this angular dispersion one of the two is lost on a structure in front of the detectors or due to its low energy it is stopped already in the target backing. Thus binary coincidences are obtained, where the *missing mass* can be Ca-isotopes, $A_3 = 48$–52 (see Ref. [14]).

It is in fact crucial for the experimental observation of these collinear ternary decays, to know the kinematic conditions for their detection. In order to clarify the experimental situation, we repeat here the results of Ref. [24] on the kinematics of the ternary collinear decay. We emphasize, that the ternary decay must be considered to occur sequentially (see Fig. 1). This is true for all ternary decays in nuclear and particle physics as discussed by Garrido et al. [22]. For our case we show in Fig. 1 our definition of the intermediate and final fragments. With this choice important quantities, e.g. the kinetic energies of the final fragments can be calculated, the results are shown in Fig. 2.

From this figure we find, that the central fragment, A_3 (which for a favored decay will be at the central position), attains extremely low kinetic energies (below 1.0 MeV), if all fragments have some intrinsic excitation energy. In the descent from the barrier to the scission point, the fragments usually attain intrinsic excitation. Thus direct experimental observation of the central fragments becomes almost impossible. Actually it may already get lost in the source-backing, thus producing binary coincidences of the outer fission fragments, with a missing mass.

From the recent work on CCT-decays and in a survey of the theoretical predictions of the last decades, see Ref. [16], it became clear, that for larger charge (mass) of the third central fragments, A_3, the ternary decay must be collinear. The collinear aligned multi-cluster pre-scission configurations are the energetically optimum configurations for ternary decays as predicted in Refs. [8, 17–19,26].
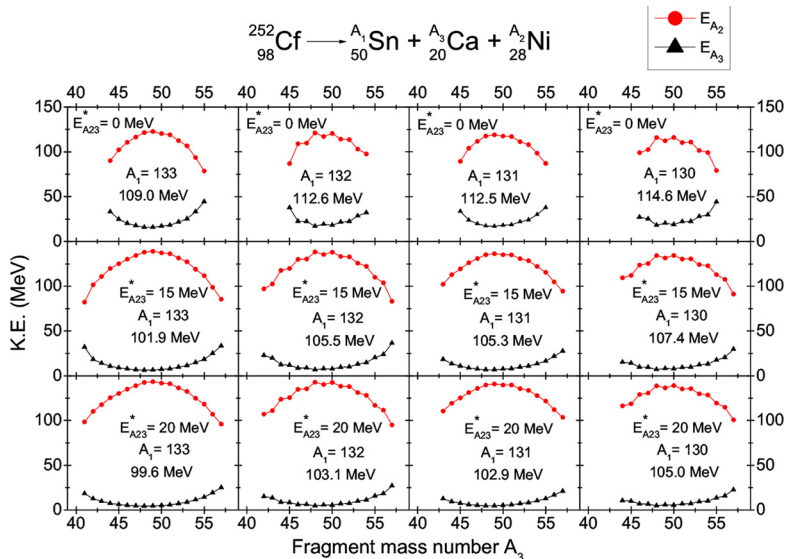

Fig. 2. The (Color online.) kinetic energies (adopted from Ref. [24]) calculated for the central fragment A_3, for different masses of A_1 for different excitation energy of A_{23} with the sequential decay as suggested in Fig. 1. In the case of excitation energies in all three fragments, the kinetic energy of the central fragment, A_3, drops to very small values.
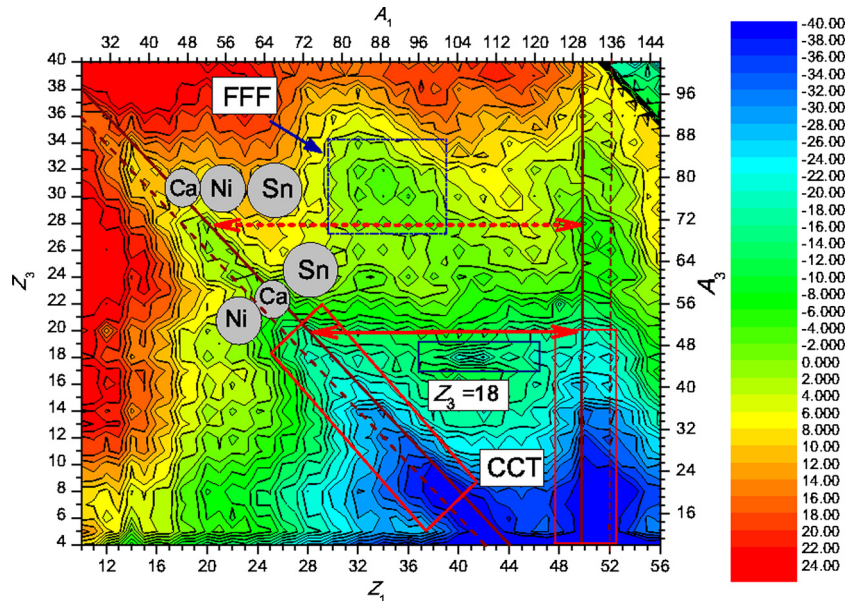
Fig. 3. (Color online.) The contour plot of the potential energy surface (PES) with an overview of the different modes for the collinear ternary decays characterized by two of the ternary fragments Z_3 and Z_1 for ^{252}Cf. The pre-scission configurations of the ternary system with the isotopes of tin, $^{132-128}$Sn, $Z_{1,2} = 50$, and Tellurium $^{134-138}$Te, $Z_{1,2} = 52$, and complimentary fragments are shown by the solid and dashed lines, respectively. The dashed rectangle shows the area of the expected mass (charge) distribution of the symmetric ternary FFF-decay products with almost equal fragment masses $A_1 \approx A_2$ and $A_3 \approx A_2$. The smaller rectangle $Z_3 = 18$ corresponds to the expected yield of the two products with close charge numbers $Z_1 = Z_2 = 40$ or $Z_1 = 38$ and $Z_2 = 42$ as described in the text. The rotated rectangle (with solid edges) and the one which is placed at the charge numbers and $Z_1 = 48-52$ show the ternary configurations leading to the collinear cluster decays (CCT), as observed in Refs. [14,15], and additional modes with smaller central fragments with $Z_3 = 6-12$, discussed in the present paper.

2. Potential energy surface (PES), internal barriers in ternary fission

The PES's are used to discuss the relative importance of the different ternary fission modes. The PES's are calculated, more details are given in Refs. [27,35], using the binding energies of the three fragments, B_1, B_2, B_3 and of the fissioning nucleus B_{CN}. With the ternary Q-value, $Q_{ggg} = B_1 + B_2 + B_3 - B_{CN}$ and the sum of interactions (nuclear and Coulomb) between all three fragments, the PES is obtained. The PES and the relative distances and the barriers are obtained in a procedure described in Ref. [27]. The relevant distances between the fragments are fixed at the value corresponding to the minimum value of the potential well obtained in the interaction potential between them (see Figs. 4 and 5). The PES is presented in Fig. 3 at the minimum values of the distances chosen among the set of PES's calculated by variation of mass numbers A_1 and A_3, with their charge numbers Z_1 and Z_3, respectively. The increase of the distances between the center of masses beyond the barrier values corresponds to scission points. The overlap of the nucleon densities is decreased and the PES is changed due to the dependence of the nucleus–nucleus interactions on the distances. The quadrupole deformation parameter of the excited first 2^+ states of nuclei, from Ref. [28], is used in the calculation of PES. The distances vary with the choice of the mass and charge numbers of the first and third fragments. The Q_{ggg}-value is determined by the structure of the three fragments and of the decaying nucleus, B_{CN}, with masses taken from the compilation of Moeller and Nix [25]. The result of the calculations for the PES's are shown as function of the masses of two fragments $A_3(Z_3)$, and $Z_1(A_1)$, in Fig. 3. With this information the phase space (see below) for the decays can be considered. We observe several dominant regions in the PES-landscape for ternary fission, defining different ternary decay modes. Clearly the favored decays are connected to specific regions with favorable phase space, which includes the Q_{ggg}-values.

From these results of the PES we also conclude, that for the originally observed CCT-decay in ^{252}Cf(sf, fff), the arrangement with Ca as a third fragment in the center, gives a lower value of the potential energy (due to the Coulomb energy). More explicitly: the arrangement of the charges with $(Z_{1,3,2}) = (28, 20, 50)$ is favored in the ternary decay relative to the arrangement with $(Z = 20, 28, 50)$ by an energy difference of about 10 MeV.

At this stage we show the results of our calculations of the internal barriers. The ingredients are basically the same as for the PES's, the variables are now the distances R_{13} and R_{23}, between the centers of the fragments A_1 and A_3, and A_2 and A_3, respectively. In particular for the CCT-mode with the central fragment $A_3 = $ Ca, two *different* barriers appear, which can be seen in the figure of the potential energies $V_{int}(R_{int}(R_{13}, R_{23}))$, shown in Fig. 4 for different modes. Here the variables are from the center-of-mass of the middle fragment "3" up to the centers-of-mass of the fragments "1" and "2", respectively. In this figure (Fig. 4) we see, that there is a systematic increase of the internal barriers as function of increasing charge/mass of the central fragment. For the lowest values of the masses (charges) of the lighter central fragment, we have the lowest barriers, the highest values appear for the symmetric decays.

The fission decay is a statistical decay mode of the nucleus [23], governed by the phase space. We have to consider several factors for the phase space of statistical decays:

i) The details of the PES, namely, the geometrical size of its dips, valleys and hills, those are related to the Q_{ggg}-values, of the decay channels,

ii) the latter determines the number of possible fragment (isotope) combinations, and

iii) the excitation energy range in the individual fragments.

There can be other dynamical factors influencing the yields [2], e.g. the formation of deformation (quadrupole and octupole) on the way from the barrier to the scission point. As a result the final
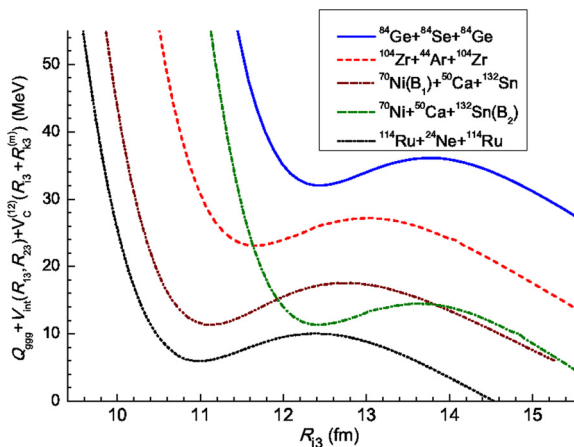
Fig. 4. (Color online.) Comparison of the internal barriers for ternary decays characterized by the charge/mass of the central fragments Z_3, and comparable masses at the two sides, for ^{252}Cf(fff). Lower barriers and higher penetrabilities appear for lighter ternary central fragments.

Fig. 5. (Color online.) Two-dimensional plot of the internal barriers for asymmetric CCT-ternary decays, characterized by the two distances R_{13} and R_{23}, and the different charge/mass of the central fragments Z_3; for ^{252}Cf. The lower barrier appears for R_{23} with the arrangement of the fragments as $A_1 + A_3 + A_2$, with (Ni + Ca + Sn).

Fig. 6. (Color online.) The experimental mass correlation ($A_{1,2} = M_{1,2}$), for the symmetric FFF-decays (adopted, modified from Ref. [34]) for ^{252}Cf using a gate with the condition on the masses $A_1 \approx A_2$ and $A_3 \approx A_2$, however, the former is the missing mass and is not observed for the symmetric FFF-decay. The arrows "FF" point to the events of the binary fission products, which have passed through the gates.

mass distribution of the fragments may change slightly from those at the pre-scission distances.

If a symmetric FFF-decay occurs, the two barriers in the sequential process will be the same (connecting the central with the heavier fragments). We observe that the internal barriers are lower for lighter central fragments: For the case of the nonsymmetric CCT-decay with three different final fragments (Ni, Ca, Sn), two barriers corresponding to the interaction of A_3 with fragment A_1 or/and with A_2 are obtained, they can be plotted in a two-dimensional contour as shown in Fig. 5.

With this information on barriers and the PES we can discuss the different decay modes. In the PES for ^{252}Cf, in Fig. 3, we find several favored regions for the ternary decays, which are due to a larger phase space for the distinct minima in various charge combinations with $\Sigma_Z = 98$.

For the purpose of comparing the modes predicted with the PES, it is useful to cite results of an experiment reported in Ref. [32] on the ^{235}U(n_{th}, ff) reaction with coincidences of fragments with γ-emissions. From this work we deduce, that for decays with light central fragments, the latter are rather neutron rich. In our case with two neck ruptures two neutrons from scission at each neck rupture may be observed. The maximum neutron emission probability in binary fission in this work is mainly due to excited fragments, it is typically in the 2n- and 3n-channels. In the cited work also average spin 8(+) values are deduced. In the next section we discuss the fragment yields observed in the different decay modes as deduced from the experiments of Refs. [14,15].

3. The multi-modal ternary decays of ^{252}Cf

1) The symmetric FFF-decay:

We have already analyzed in a previous publication, Ref. [34], one of the important ternary fission modes ("true ternary fission") predicted by the PES with *almost equal fragment masses*, with $A_1 \approx A_2$, and $A_3 \approx A_2$, which we will call FFF. This symmetric decay with e.g. ^{84}Ge + ^{84}Se + ^{84}Ge ($Z_1 = 32, 34$, or 32) and ($Z_3 = (30, 32, 34)$), the fragment Z_2 has an equivalent role and the values of $Z_2 = 32, 34$, are similar to the first two (of Z_1, Z_3). For the experimental data, we select events with the conditions on the masses $A_1 \approx A_2$ and in principle also $A_3 \approx A_1$, however, A_3 is the missing mass (not observed). This is a symmetric decay, the result is shown in Fig. 6 (from Ref. [34]).

In this experiment the background due to the scattering tails from the support grids in the FOBOS-detectors and other ternary
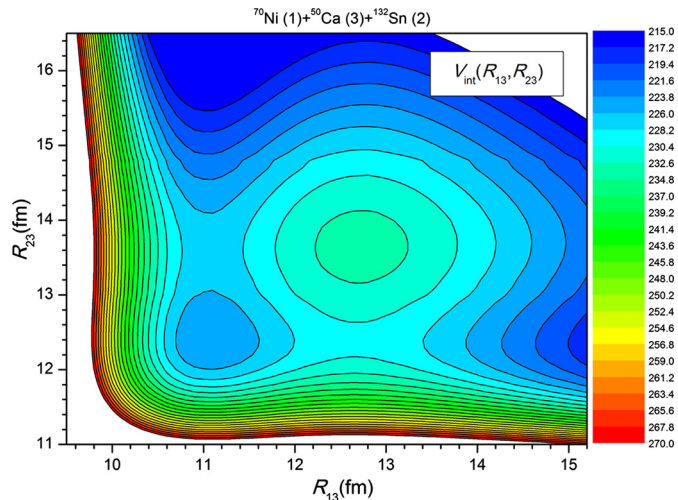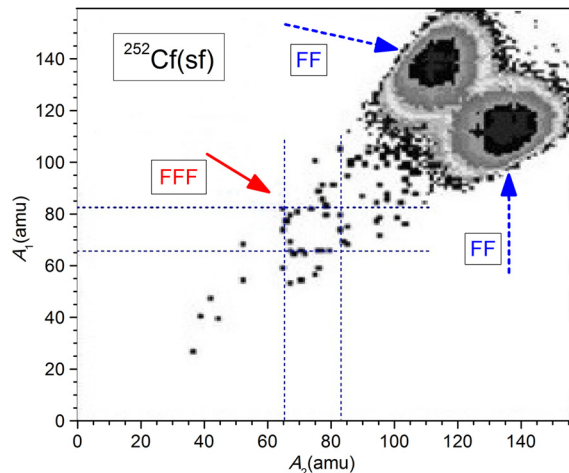
decay modes, has disappeared in the data. The yield (relative to binary decays) for the symmetric FFF-decay is found to be in the range of $2 \cdot 10^{-6}$/(binary fission), as reported in Ref. [34]. This decay has been expected to have a yield, that is 5 orders of magnitude lower than for binary FF, as discussed in Ref. [19].

For the deformation effects, they mostly are contained in the ground state masses. The dependence of nuclear shell effects on deformation in the fragments is quite important. A full appraisal of such effects, where many mass and charge combinations of the three fragments enter, needs a larger effort. We have restricted our calculations to the information contained in the ground state binding energies and the use of deformation parameters of the 2^+ states. The fact that we have three fragments with binding energies close to the maximum of the overall values of the (binding energy)/nucleon, gives a large effect in the Q_{ggg}-values, this results in large Q-values and deeper holes in the PES. The Q_{ggg}-value for this symmetric FFF-decay in ^{252}Cf(sf, FFF) is $Q_{FFF} = 268.3$ MeV. This value is higher then for the previously observed CCT-decay

with $Q_{CCT} = 250.6$ MeV, and much higher than those for binary decays, which have values in the region with $Q_{binary} = 205$ MeV.

2) The asymmetric CCT-decay:

This originally observed ternary decay has been discussed in Refs. [14,15]. From the PES we see two possibilities: i) for CCT with $Z_3 = 20$, and $Z_1 = 28$ and ii) less pronounced for $Z_3 = 28$, and $Z_1 = 20$. The complementary fragments with Z_2 are isotopes of Sn ($Z = 50$). From the experiments reported in Refs. [14,15] an overall yield of $4 \cdot 10^{-3}$/(binary fission), contained in a larger bump of fragment mass combinations, has been observed. The energy level (seen in the PES in Fig. 3) of $(28 + 20 + 50)$, $Z_3 = 20$, and $Z_1 = 28$, and $Z_2 = 50$ is lower compared to $(20 + 28 + 50)$ with $Z_3 = 28$.

For the potentials, shown in Fig. 4, the dashed and dot-dashed curves correspond to this channel. Note, these curves present the total energy as a sum of the reaction Q_{ggg}-value and the interactions between fragments. The corresponding internal barriers are low, see Fig. 4. In a two steps model, the first step proceeds through the lowest barrier. The separation barrier for the Z_3, and the ^{132}Sn fragment, is determined by the depth of the potential-well shown by the dotted curve in Fig. 4, it is lower than the one for the separation with fragment Z_1 (^{70}Ni).

With the large Q-values of the ternary mass partitions (e.g. 251.37 MeV, for ^{132}Sn + ^{50}Ca + ^{70}Ni) in the CCT events, many fragment combinations (with a variation of neutron numbers) are formed producing a bump like in the data observed in binary fission. The phase space is discussed in a study of the kinematics for the collinear breakup into isotopes of (Sn + Ca + Ni) in Ref. [24]. A sequential decay is assumed with two neck ruptures. With the information from Ref. [22] we conclude, that the first step goes through the lower of the two barriers. The same assumptions apply to the FFF-decays, the time sequence of the two random (in time) neck-ruptures is connected to the binary fission times. Actually, proceeding for FFF-decays as in Ref. [24], we find that the kinetic energy of the central fragment (with some excitation energy in all fragments) in FFF-decay will have values close to zero! Therefore, *in the FFF-decay the central fragment may be stopped in the target or/and in the backing pointing to arm1*, leading to binary coincidences with a missing mass of $A_3 = 70$–80.

3) Decays with $Z_3 = 18$:

To our surprise the PES in Fig. 3 for ^{252}Cf(sf, fff), suggests ternary decay modes (pronounced minima), for charge combinations with $Z_3 = 18$, and $Z_1 = 40, 42$ (for masses ($^{46-44}$Ar and ^{104}Zr + ^{102}Zr and/or ^{106}Mo). Such an effect is also seen in the PES for ^{236}U shown in Ref. [34]. A strong yield of fragment combinations with ^{46}Ar ($Z_3 = 18$) and with ^{26}Ne is expected. We refer to the special shell structure described in Refs. [29,30], for the neutron rich isotopes $^{44-46}$Ar and ^{26}Ne. The dominating effect comes from the shell properties of the central smaller fragments. For the visualization and extraction of the yield, we use the fact that the continuum observed in binary coincidences in the range of smaller masses, contains ternary decays. In this case two fragments (of three) moving into the direction of arm1, have due to scattering in the target backing an angular dispersion with the blocking of one of the fragments, see Ref. [14], where this effect is described. This introduces a loss of one (out of three) fragment in the ternary events. In the total mass spectrum particular masses are removed by this method, giving a dip in the originally continuous spectrum. The result with this method is discussed also in Ref. [33] and illustrated in Fig. 7. The two spectra of arm1 and arm2 are shown (part a), with the second derivative of the spectrum of arm1 shown in Fig. 7 (part b). The windows w1 and w2 are chosen to remove background. The second derivative shows the extra missing events in the range of masses of $M_1 = 102$–112 in the continuum (distorted, and shifted due to the contribution of the ternary decays).
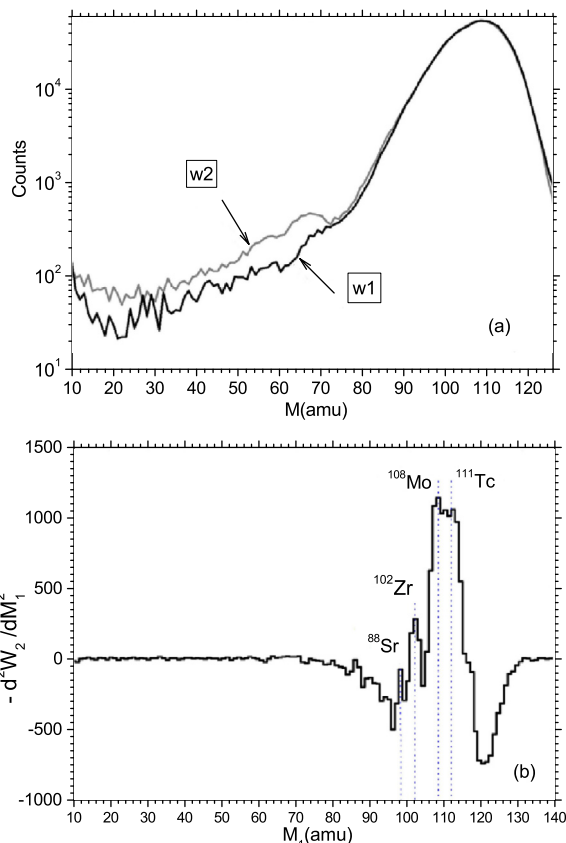

Fig. 7. (Color online.) The almost symmetric FFF-decays from the data of Ref. [15] for ^{252}Cf, for the symmetric decay with $A_3 = (^{44}$Ar), and with the restriction to the masses $A_1 \approx A_2$. a) the projections of the events from box $w1$ and box $w2$ onto M1 and M2 axes, respectively; b) the second derivative (taken with negative sign) of the spectrum being the projection of the events from box $w2$ onto M1 axis.

Also the properties of the *Mo-isotopes* are remarkable, see the recent discussion in Ref. [31]. In a binary coincidence study of the formation of the pair ^{106}Mo + ^{144}Ba (with two neutrons missing), this isotope ^{106}Mo has the highest yield. There is a sharp transition from spherical to prolate deformation in the region of $A = 102$ (spherical) to $A = 106$ (deformed with $Q = 5$ barn). The latter appears favorable for the elongated fission shape populated in this ternary decay.

4) Decays with lighter ternary central fragments:

Inspecting the PES we expect high yields for lower values of Z_3, see Fig. 3. Here an area of favored potential energies in the PES for ternary decays appears with $Z_3 = 12, 10, 8, 6$, corresponding to masses $M_3 = 34$–14, which are combined in the PES with values of $Z_1 = 36$–42 and with masses $M_1 = 68$–90. This gives us for the complementary masses of fragment M_2, values in the range $M_2 = 132$–148.

In the data from the experiment with the neutron-coincidences, e.g. for $(n = 2)$, we find in Fig. 8 in the two-dimensional plot of the data, the coincidences of the two heavier fragments M_1 and M_2, with M_3 as the missing fragment: combining $M_1 = 68$–90 with $M_2 = 132$–148 the main concentration of events in the correlation plot is as predicted in this region (Fig. 8 adopted, modified from Ref. [15]).

These areas in the experimental correlation plot with $(n = 2)$ relate to decays with missing lighter fragments as central nuclei with *neutron-rich* isotopes of Ne, O, and C. In fact, with these lighter fragments we anticipate an increased neutron emission from the *two neck-ruptures*, with two heavier fragments at the outside borders of the chains. The projection onto the axis with M1 is
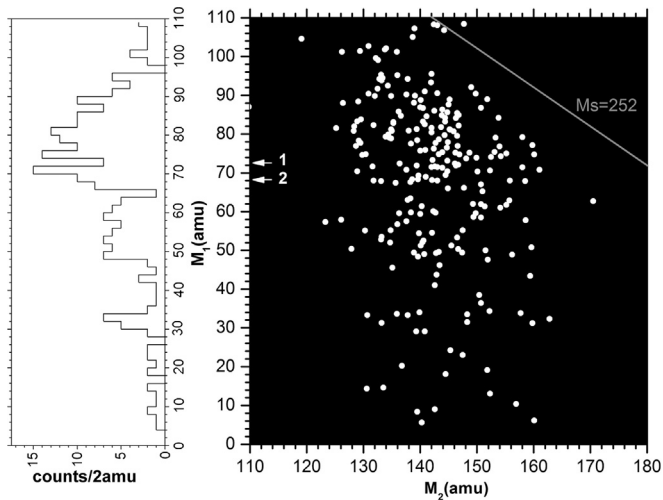
Fig. 8. The experimental binary mass correlation from fission decays for ^{252}Cf with a neutron multiplicity of $n = 2$ from the data of Ref. [15]. This frame shows the region with smaller values of missing mass or charge, $Z_3 = 6\text{--}12$ (with mass ranges $M_1 = 0\text{--}100$ and $M_2 = 100\text{--}180$).

also shown. In this work in Ref. [15], the neutron detectors have been arranged perpendicular to the fission axis of the binary coincidences, defined by the two arrays of pin-diodes. This orientation has been chosen to have an increased efficiency for the spontaneous neutrons emitted during fission, potentially from the two necks with the lighter fragments.

In these binary correlation data observed in coincidences with neutrons ($n = 2$) in Fig. 8, we observe that the background seen in the region of the correlation plot (M_1, M_2) in Ref. [14], has disappeared. We can conclude that a larger variety of ternary decays with smaller fragments (Z_3) occurs. As examples we have $(Z_3 + (Z_2 + Z_1) = 6 + (40 + 46)$, $(Z_3 + (Z_2 + Z_1) = 8 + (38 + 46)$, $(Z_3 + (Z_2 + Z_1)) = 10 + (42 + 46)$, etc., filling the region in the PES with the lower values of Z_3. If we compare the different ternary decay yields presented here with those of Ref. [4], we have to be aware of the fact that the "ternary fission" discussed in Ref. [4], refers to single isotopes with potentially one excited state. Thus the phase space for these collinear ternary decay modes are quite different, the true ternary fission in our definition usually contains several isotopes (see also Ref. [24]).

In order to judge the absolute yield of these events we have to refer to work cited in Ref. [15]. We discuss the yields of ternary relative to binary fission channels. According to the higher barriers for FFF-decays, we expect a much smaller total probability for FFF-decays compared to the originally observed CCT-decay in Ref. [14]. From the events attributed to the FFF decay shown in Fig. 6 we obtain an overall probability of $4.0 \cdot 10^{-6}$/(binary fission), namely aprox. 100–1000 times smaller then observed for the original CCT decay, of ($4.1 \cdot 10^{-3}$), as cited in Ref. [14].

For the determination of the absolute yields of the decays with smaller values of (Z_3) and ($n = 2$) we have to know the overall efficiency for neutron coincidences with the multiplicity ($n = 2$) in the data of Fig. 8. For the absolute values there is some uncertainty of the filter with the neutron-multiplicity of ($n = 2$). The efficiency for ($n = 2$) for a central source can be estimated. Higher values of the multiplicity can also contribute to this filter. Actually the original multiplicity in these modes may be as high as ($n = 4$). The necessary information is given in Ref. [15]. The geometric efficiency (solid angle) for neutrons emitted isotropically from the center, is $= 0.29$, the total efficiency of the neutron detectors is then 0.12% this implies for ($n = 2$) a factor 0.0144. For neutrons with binary fission fragments this is 5%.

For 10 counts of primary events, the data in this field, will have 8333 counts in the center of mass, in the coincident correlation plot of Fig. 8, this gives for the ratio ternary/binary (FFF/FF $=$ (0.0012)). Corresponding to a value of $2.1 \cdot 10^{-3}$ probability in ternary fissions per binary. Other modes with $Z_3 = 6, 8, 10$, will have yields of approx. $5.0 \cdot 10^{-3}$/binary. For these modes, the fact that the internal barriers are lower, explains the higher yields compared to the CCT-yields cited in Refs. [14,15].

We conclude that in the data of Refs. [14,15] several modes of collinear ternary fission are contained, with a larger variation of neutron numbers (see Ref. [15]). We refer to these as *multimodal ternary fission*, determined by the properties of the PES. As suggested by the calculations for the internal barriers, there appears a systematic evolution of the yields, with the variation of the mass of the central fragment. We have decreasing internal barriers as function of the decreasing masses (charge) of the third central fragment, and correspondingly an increasing yield for those modes. The relative probability to binary decay of these various ternary decays are in the range of $2.1 \cdot 10^{-3}$ to $1.0 \cdot 10^{-6}$. The different modes are independent from each other, they are observed simultaneously with the fragmentations in the CCT-mode first reported in Ref. [14]. A treatment of these decays with the statistical model will be given in Ref. [35].

Acknowledgements

References

[1] O. Hahn, F. Strassmann, Naturwissenschaften 46 (1939) 89.
[2] C. Wagemans (Ed.), The Nuclear Fission Process, CRC Press Inc., 1991.
[3] As Ref. [2], p. 574.
[4] F. Gönnenwein, Nucl. Phys. A 734 (2004) 213.
[5] F. Gönnenwein, Europhys. News 36 (1) (2005) 11.
[6] W.J. Swiatecki, in: Proceedings of the Second UN Conference on the Peaceful Uses of Atomic Energy, vol. 15, Geneva, 1958, United Nations, Geneva, 1958, p. 651.
[7] V.M. Strutinsky, et al., Nucl. Phys. 46 (1963) 639.
[8] D.N. Poenaru, R.A. Gherghescu, W. Greiner, Nucl. Phys. A 747 (2005) 182–205.
[9] V.I. Zagrebaev, A.V. Karpov, W. Greiner, Phys. Rev. C 81 (2010) 044608;
Also V. Zagrebaev, W. Greiner, in: C. Beck (Ed.), Clusters in Nuclei, vol. 1, in: Lect. Notes Phys., vol. 818, Springer, Heidelberg, Berlin, 2010, pp. 267–315, Chapter 7.
[10] G. Adamian, N. Antonenko, W. Scheid, in: C. Beck (Ed.), Lect. Notes Phys., vol. 848, 2012, pp. 165–227, vol. 2.
[11] D. Poenaru, W. Greiner, in: C. Beck (Ed.), Lect. Notes Phys., vol. 818, 2010, pp. 1–56, vol. 1.
[12] M.G. Itkis, I.M. Itkis, G.N. Knyazhevaa, E.M. Kozulin, Nucl. Phys. A 834 (2010) 1–4, and refs.
[13] L. Ghys, A.N. Andreev, M. Huyse, et al., Phys. Rev. C 90 (2014) 041301(R).
[14] Yu.V. Pyatkov, et al., Eur. Phys. J. A 45 (2010) 29.
[15] Yu.V. Pyatkov, et al., Eur. Phys. J. A 48 (2012) 94.
[16] W. von Oertzen, Y.V. Pyatkov, D. Kamanin, in: Zakopane Conference, Acta Phys. Pol. B 44 (2013) 447.
[17] H. Diehl, W. Greiner, Nucl. Phys. A 229 (1974) 29.
[18] G. Royer, J. Phys. G, Nucl. Part. Phys. 18 (1992) 1992.
[19] K. Manimaran, et al., Phys. Rev. C 83 (2011) 034609.
[20] M. Csatlos, A. Krasnahorkay, P.G. Thirolf, et al., Phys. Lett. B 615 (2005) 175.
[21] P. Schall, et al., Phys. Lett. B 191 (1987) 339.
[22] E. Garrido, et al., Nucl. Phys. A 748 (2005) 27;
E. Garrido, et al., Nucl. Phys. A 766 (2006) 74.
[23] N. Bohr, J.A. Wheeler, Phys. Rev. 56 (1939) 426.
[24] K.R. Vijayaraghavan, W. von Oertzen, M. Balasubramaniam, Eur. Phys. J. A 48 (2012) 27.

[25] P. Moeller, J.R. Nix, W.D. Meyers, W.J. Swiatecki, At. Data Nucl. Data Tables 59 (1995) 185.
[26] K.R. Vijayaraghavan, M. Balasubramaniam, W. von Oertzen, Phys. Rev. C 90 (2014) 024601.
[27] R.B. Tashkhodjaev, A.K. Nasirov, W. Scheid, Eur. Phys. J. A 47 (2011) 136.
[28] S. Raman, C.W. Nestor Jr., P. Tikkanen, At. Data Nucl. Data Tables 78 (2001) 1.
[29] B. Fornal, R. Broda, R.W. Krolas, et al., Eur. Phys. J. A 7 (2000) 147.
[30] O. Sorlin, Nucl. Phys. A 685 (2001) 186c–197c.
[31] R. Roddriguez-Guzmaná, et al., Phys. Lett. B 691 (2010) 202.
[32] S. Mukhopadhyay, et al., Phys. Rev. C 85 (2012) 064321.
[33] D. Kamanin, Y.V. Pyatkov, in: C. Beck (Ed.), Clusters in Nuclei, vol. 3, in: Lect. Notes Phys., vol. 875, Springer, Heidelberg, Berlin, 2014, pp. 183–246, Chapter 6.
[34] W. von Oertzen, A.K. Nasirov, Phys. Lett. B 734 (2014) 234.
[35] R.B. Tashkhodjaev, A.I. Muminov, A.K. Nasirov, W. von Oertzen, Y. Oh, Phys. Rev. C (2015), in press, arXiv:1503.03158.